analytica

MDPI

Article

Using Hydrogen/Deuterium Exchange in Untargeted LC-MS Analysis of Small Molecules

Tomas Cajka [1,*], Jiri Hricko [1], Lucie Rudl Kulhava [1], Veronika Hola [1], Michaela Paucova [1], Michaela Novakova [1] and Oliver Fiehn [2]

[1] Institute of Physiology of the Czech Academy of Sciences, Videnska 1083, 14200 Prague, Czech Republic; jiri.hricko@fgu.cas.cz (J.H.); lucie.kulhava@fgu.cas.cz (L.R.K.); veronika.hola@fgu.cas.cz (V.H.); michaela.paucova@fgu.cas.cz (M.P.); michaela.novakova@fgu.cas.cz (M.N.)

[2] West Coast Metabolomics Center, UC Davis Genome Center, University of California, 451 Health Sciences Drive, Davis, CA 95616, USA; ofiehn@ucdavis.edu

* Correspondence: tomas.cajka@fgu.cas.cz

Abstract

Liquid chromatography–hydrogen/deuterium exchange–mass spectrometry (LC-HDX-MS) provides orthogonal structural information that complements conventional LC-MS and improves confidence in small-molecule structural elucidation. Although HDX-MS is well established in protein research, its application to small molecules remains less developed, and practical guidance for experimental implementation and data interpretation is limited. Here, we evaluate major LC-HDX-MS strategies, including post-column co-infusion, partial HDX, and full HDX approaches, and assess their analytical performance using reference standards and NIST SRM 1950 human plasma. The effects of deuterated mobile phases on background contamination, labeled/unlabeled signal ratios, retention-time shifts, adduct chemistry, and mass spectral interpretation are examined, and currently available software tools for LC-HDX-MS data processing are discussed. Full HDX provided the most complete deuterium incorporation, whereas deuterated mobile phases increased background signals and generally reduced analyte responses. Retention-time shifts were typically small but should be considered when matching features. HDX-derived information provides an additional experimental structural descriptor by defining the number of exchangeable hydrogen atoms and refining adduct assignments, thereby reducing ambiguity during structural annotation. These findings provide practical recommendations for implementing LC-HDX-MS in untargeted LC-MS workflows and demonstrate its value as an orthogonal tool for small-molecule structural elucidation.

Keywords: metabolomics; lipidomics; exposomics; LC-MS; hydrogen/deuterium exchange; structural elucidation

Academic Editor: Marcello Locatelli

Received: 26 June 2026
Revised: 30 July 2026
Accepted: 18 August 2026
Published: 20 August 2026

1. Introduction

Liquid chromatography–mass spectrometry (LC-MS) has become an indispensable analytical platform in untargeted metabolomics, lipidomics, and exposomics [1–3]. Continuous improvements in chromatographic separations, high-resolution mass spectrometry, and computational data processing have substantially expanded analytical coverage and sensitivity [4–8]. Nevertheless, reliable structural elucidation of small molecules remains challenging. Isomeric complexity, diverse adduct formation, variable ionization behavior, and limited fragmentation specificity frequently lead to ambiguous annotations and elevated false-positive rates in untargeted workflows [9].

Hydrogen/deuterium exchange mass spectrometry (HDX-MS) provides an additional layer of structural information that can complement conventional LC-MS analysis. While HDX approaches are well established in protein structural biology [10,11], their adaptation to small-molecule analysis has gained increasing attention only in recent years [12–26]. HDX for small-molecule analysis can be implemented using several experimental configurations. Beyond LC-based workflows, HDX has been performed in solution prior to analysis, through post-column solvent mixing [12,27], within microdroplets [28], in the gas phase [29,30], and in combination with imaging MS [31,32] or ion mobility spectrometry [18]. These approaches differ in exchange mechanisms, timescales, instrumentation requirements, and the type of structural information obtained. Depending on the experimental design, structural information may be derived from either forward H/D exchange or controlled H/D back-exchange processes [22]. In LC-HDX-MS workflows, exchangeable hydrogen atoms are replaced with deuterium during chromatographic separation or via post-column mixing, producing characteristic mass shifts governed by molecular structure, ionization chemistry, and adduct formation [33,34].

Exchangeable hydrogen atoms are typically those attached to heteroatoms, most commonly oxygen, nitrogen, and sulfur atoms in hydroxyl, carboxyl, amino, amide, thiol, and phosphate groups, that undergo hydrogen/deuterium exchange under the applied experimental conditions [34]. Under certain conditions, however, additional hydrogen atoms may become exchangeable through processes such as keto–enol tautomerization [35]. The extent of exchange depends on both the molecular structure and the experimental conditions, including solvent composition, pH, ionization mode, and exchange time [11,22,36,37]. Consequently, the experimentally observed number of exchanged hydrogen atoms should be interpreted as an experimental descriptor that reflects both the molecule's intrinsic exchangeability and the LC-HDX-MS conditions under which the analysis is performed.

When combined with accurate mass, retention time, isotope patterns, adduct assignment, and MS/MS spectra, the experimentally determined number of exchanged hydrogen atoms provides an additional structural descriptor that complements conventional LC-MS data and can substantially increase confidence in small-molecule structural elucidation [38]. Rather than replacing established annotation workflows, HDX-derived information serves as orthogonal experimental evidence to help distinguish candidate structures that remain ambiguous after conventional LC-MS analysis.

Here, we present a practical evaluation of LC-HDX-MS for untargeted metabolomics and lipidomics, focusing on experimental implementation and interpretation of HDX-derived structural information. Using reference standards and human plasma samples, we evaluate different HDX strategies, deuterated mobile phases, retention-time behavior, labeled/unlabeled signal ratios, adduct chemistry, mass spectral interpretation, and available data-processing workflows. Based on these observations, we provide practical recommendations for experimental design and discuss how LC-HDX-MS can be integrated with conventional LC-MS workflows to improve confidence in small-molecule structural elucidation.

2. Materials and Methods

2.1. Reagents for LC-MS

For sample extraction, LC-MS-grade methanol (J.T.Baker, Phillipsburg, NJ, USA) and water (VWR, Suwanee, GA, USA) were used, while methyl *tert*-butyl ether (MTBE) (Honeywell, Charlotte, NC, USA) was HPLC-grade. LC-MS-grade solvents for mobile phases included acetonitrile (Honeywell), methanol (J.T.Baker), isopropanol (Supelco, Darmstadt, Germany), and water (VWR). Mobile-phase modifiers, such as ammonium

formate (Supelco), ammonium acetate (Sigma–Aldrich, Darmstadt, Germany), formic acid (VWR), and acetic acid (VWR), were also LC-MS-grade.

For HDX-MS experiments, formic acid-D_2 (Sigma–Aldrich), acetic acid-D_4 (CIL, Tewksbury, Massachusetts, USA), ammonium formate-D_5 (Sigma–Aldrich), ammonium acetate-D_7 (Sigma–Aldrich), deuterium oxide (Sigma–Aldrich), methanol-D_4 (Sigma–Aldrich), and isopropanol-D_8 (ARMAR, Döttingen, Switzerland) were used.

Reference standards (amino acid mix, Val-Tyr-Val) were obtained from Sigma–Aldrich, while 12-[[(cyclohexylamino)carbonyl]amino]-dodecanoic acid (CUDA) was from Cayman Chemical (Tallinn, Estonia). Reference standards of lipids (PC 15:0/18:1-d_7, LPC 17:1, SM 18:1; O2/17:0, Cer 18:1; O2/17:0, CL 16:0/16:0/16:0/16:0, PE 17:0/17:0, PG 17:0/17:0, LPE 17:1, PS 17:0/17:0, SPB 17:1; O2, GlcCer 18:1; O2/17:0) were from Sigma–Aldrich. Human plasma reference material NIST SRM 1950 (Sigma–Aldrich) was used.

2.2. Sample Extraction

For the sample extraction, a biphasic solvent system of methanol, MTBE, and water was used (LIMeX workflow) [39,40]. Plasma samples were thawed before pipetting.

Plasma samples (25 µL) were mixed with 165 µL of cold methanol, shaken (30 s), mixed with 600 µL of cold MTBE, and shaken (30 s) again. Then, 165 µL of 10% methanol was added, and the tubes were vortexed (20 s) and centrifuged (16,000 rpm, 10 min, 4 °C).

The first aliquot of 70 µL of the bottom phase was collected and evaporated to analyze polar metabolites. The dry extracts were resuspended in 70 µL of an acetonitrile/water (4:1) mixture, shaken (30 s), centrifuged (16,000 rpm, 5 min, 4 °C), and analyzed using the hydrophilic interaction liquid chromatography (HILIC) metabolomics platforms in positive electrospray ionization (ESI) mode. For HILIC-HDX-MS experiments, the dry extracts were resuspended in 70 µL of an acetonitrile/D_2O (4:1) mixture.

The second 70 µL aliquot of the bottom phase was mixed with 210 µL of an isopropanol/acetonitrile (1:1) mixture to precipitate residual proteins, shaken (30 s), and centrifuged (16,000 rpm, 5 min, 4 °C), and the supernatant was evaporated. The dry extracts were resuspended in 5% methanol/95% water/0.2% formic acid, shaken (30 s), centrifuged (16,000 rpm, 5 min, 4 °C), and analyzed using the reversed-phase liquid chromatography (RPLC) metabolomics platform in negative ESI mode. For metabolomics RPLC-HDX-MS experiments, the dry extracts were resuspended in 70 µL of a 5% methanol-D_4/95% D_2O/0.2% formic acid-D_2 mixture.

A 200 µL aliquot of the upper phase was collected and evaporated to analyze complex lipids. The dry extracts were resuspended in 100 µL of methanol, shaken (30 s), centrifuged (16,000 rpm, 5 min, 4 °C), and analyzed using the RPLC lipidomics platforms in positive and negative ESI mode. For lipidomics RPLC-HDX-MS experiments, the dry extracts were resuspended in 100 µL of methanol-D_4.

2.3. LC-MS Analysis

For LC-MS analysis, a Vanquish UHPLC system (Thermo Fisher Scientific, Waltham, MA, USA), a heated ESI (HESI-II) probe (Thermo Fisher Scientific), and a Q Exactive Plus mass spectrometer (Thermo Fisher Scientific) were used [39,40].

2.3.1. LC-MS-Based Metabolomics

The mobile-phase modifiers were selected based on previously optimized metabolomics methods developed in our laboratory [39], providing an optimal balance between chromatographic performance, analyte response, and retention-time stability for the respective ionization modes.

For the separation of polar metabolites based on the HILIC mechanism, the following conditions were used: an ACQUITY Premier BEH Amide column (50 mm length × 2.1 mm

i.d.; 1.7 µm particle size) with a VanGuard FIT cartridge (5 mm length × 2.1 mm i.d.; 1.7 µm particle size) (Waters); column compartment temperature, 45 °C; column flow rate, 0.4 mL/min; mobile phase A, water with 10 mM ammonium formate and 0.125% formic acid; mobile phase B, acetonitrile/water (95:5) with 10 mM ammonium formate and 0.125% formic acid; gradient run, 0 min 100% B, 0–1 min 100% B, 1–3.9 min from 100% to 70% B, 3.9–5.1 min from 70% to 30% B, 5.1–6.4 min from 30% to 100% B, 6.4–7.5 min 100% B +1 min preinjection steps; injection volume, 1 µL.

For HILIC-HDX-ESI(+)-MS experiments, the mobile phases were: mobile phase A, D_2O with 10 mM ammonium formate-D_5 and 0.125% formic acid-D_2; mobile phase B, acetonitrile/D_2O (95:5) with 7.5 mM ammonium formate-D_5 and 0.125% formic acid-D_2 [12]. The 7.5 mM ammonium formate-D_5 concentration was a limiting factor when D_2O was used as part of mobile phase B, as ammonium formate-D_5 was not fully soluble at concentrations greater than 7.5 mM [12].

For the separation of polar metabolites based on the RPLC mechanism, the following conditions were applied: an ACQUITY Premier HSS T3 column (50 mm length × 2.1 mm i.d.; 1.8 µm particle size) with a VanGuard FIT cartridge (5 mm length × 2.1 mm i.d.; 1.8 µm particle size) (Waters); column compartment temperature, 45 °C; mobile phase A, water with 0.2% formic acid; mobile phase B, methanol with 0.1% formic acid; gradient run and column flow, 0 min 1% B 0.3 mL/min, 0–0.5 min 1% B 0.3 mL/min, 0.5–2 min from 1% to 60% B 0.3 mL/min, 2–2.3 min from 60% to 95% B from 0.3 mL/min to 0.5 mL/min, 2.3–3.0 min 95% B 0.5 mL/min, 3.0–3.1 min from 95% to 1% B 0.5 mL/min, 3.1–4 min 1% B 0.5 mL/min, 4–4.1 min 1% B from 0.5 mL/min to 0.3 mL/min, 4.1–4.5 min 1% B 0.3 mL/min +1 min preinjection steps; injection volume, 5 µL; sample temperature, 4 °C.

For metabolomics RPLC-HDX-ESI(–)-MS experiments, the mobile phases were: mobile phase A, D_2O with 0.2% formic acid-D_2; mobile phase B, methanol-D_4 with 0.1% formic acid-D_2 [41].

The ion source parameters were: sheath gas pressure, 50 arbitrary units (a.u.); aux gas flow, 13 a.u.; sweep gas flow, 3 a.u.; capillary temperature, 260 °C; aux gas heater temperature, 425 °C; spray voltage: 3.6 kV for ESI(+), −2.5 kV for ESI(−); S-lens RF level, 50. The MS settings were: MS1 mass range, m/z 60–900; MS1 resolving power, 35,000 FWHM; AGC target, 10^6; maximum IT, 100 ms; spectrum data type, centroid; the number of data-dependent scans per cycle, 3; MS/MS resolving power, 17,500 FWHM; AGC target, 10^5; maximum IT, 50 ms; spectrum data type, centroid; isolation window, 1 m/z; minimum AGC target, 10^3; dynamic exclusion, 2 s; exclude isotopes, on; normalized collision energies: 20, 30, and 40%.

2.3.2. LC-MS-Based Lipidomics

The mobile-phase additives were optimized separately for positive- and negative-ionization lipidomics based on our previous methodological evaluation [39]. Ammonium formate with formic acid was used for ESI(+), whereas ammonium acetate with acetic acid was used for ESI(−), providing the best overall compromise between lipid signal intensity, chromatographic performance, and retention-time stability.

For the separation of complex lipids based on the RPLC mechanism, the following conditions were applied: an ACQUITY Premier BEH C18 column (50 mm length × 2.1 mm i.d.; 1.7 µm particle size) with an with a VanGuard FIT cartridge (5 mm length × 2.1 mm i.d.; 1.7 µm particle size) (Waters); column compartment temperature, 65 °C; column flow rate, 0.6 mL/min; mobile phase A for ESI(+), 60:40 acetonitrile/water with 10 mM ammonium formate and 0.1% formic acid; mobile phase B for ESI(+), 90:10:0.1 isopropanol/acetonitrile/water with 10 mM ammonium formate and 0.1% formic acid; mobile

phase A for ESI(−), 60:40 acetonitrile/water with 10 mM ammonium acetate and 0.1% acetic acid; mobile phase B for ESI(−), 90:10:0.1 isopropanol/acetonitrile/water with 10 mM ammonium acetate and 0.1% acetic acid; gradient run for ESI(+), 0 min 15% B, 0–1 min from 15% to 30% B, 1–1.3 min from 30% to 48% B, 1.3–5.5 min from 48% to 82% B, 5.5–5.8 min from 82% to 99% B, 5.8–6 min 99% B, 6–6.1 min from 99% to 15% B, 6.1–7 min 15% B +1 min preinjection steps; gradient run for ESI(−), 0 min 15% B, 0–1 min from 15% to 30% B, 1–1.3 min from 30% to 48% B, 1.3–4.8 min from 48% to 76% B, 4.8–4.9 min from 76% to 99% B, 4.9–5.3 min 99% B, 5.3–5.4 min from 99% to 15% B, 5.4–6.3 min 15% B +1 min preinjection steps; injection volume, 1.5 µL for ESI(+), 5 µL for ESI(–); sample temperature, 4 °C.

For lipidomics RPLC-HDX-ESI(+)-MS experiments, the mobile phases were: mobile phase A, 60:40 acetonitrile/D_2O with 10 mM ammonium formate-D_5 and 0.1% formic acid-D_2; mobile phase B, 90:10:0.1 isopropanol-D_8/acetonitrile/D_2O with 10 mM ammonium formate-D_5 and 0.1% formic acid-D_2. For lipidomics RPLC-HDX-ESI(–)-MS experiments, the mobile phases were: mobile phase A, 60:40 acetonitrile/D_2O with 10 mM ammonium acetate-D_7 and 0.1% acetic acid-D_4; mobile phase B, 90:10:0.1 isopropanol-D_8/acetonitrile/D_2O with 10 mM ammonium acetate-D_7 and 0.1% acetic acid-D_4.

The ion source parameters were as follows: sheath gas pressure, 60 a.u.; aux gas flow, 25 a.u.; sweep gas flow, 2 a.u.; capillary temperature, 300 °C; aux gas heater temperature, 370 °C; spray voltage for ESI(+), 3.6 kV; spray voltage for ESI(−), −3.0 kV; S-lens RF level, 50. The MS settings were: MS1 mass range, m/z 200–1700; MS1 resolving power, 35,000 FWHM; AGC target, 10^6; maximum IT, 100 ms; spectrum data type, centroid; the number of data-dependent scans per cycle, 3; MS/MS resolving power, 17,500 FWHM; AGC target, 10^5; maximum IT, 50 ms; spectrum data type, centroid; isolation window, 1 m/z; minimum AGC target, 10^3; dynamic exclusion, 2 s; exclude isotopes, on; normalized collision energy in ESI(+), 20%; normalized collision energies in ESI(−), 10, 20, and 30%.

2.4. Data Processing

All the LC-MS raw files were converted into mzML format using ProteoWizard software v. 3.0.22342 (https://proteowizard.sourceforge.io accessed on 10 December 2025) [42].

MS-DIAL v. 5.5.260323 (https://github.com/systemsomicslab/MsdialWorkbench/releases/tag/MSDIAL-v5.5.260323 accessed on 29 May 2026) was used to process converted LC-MS files, including peak detection, deconvolution, alignment, and annotation of test compounds [43]. The following parameters were used: (i) data collection: MS1 tolerance, 0.001; MS2 tolerance, 0.01; maximum number of isotopes, 3; consider Cl and Br elements, checked; (ii) peak detection: minimum peak height: 15,000; mass slice width, 0.001; smoothing method, Linear Weighted Moving Average; smoothing level, 3; (iii) MZRT identification setting: accurate mass tolerance (MS1), 0.002; retention time tolerance, 0.05 min; use retention time for filtering, checked; (iv) alignment: retention time tolerance: 0.05 min; MS1 tolerance: 0.002 Da; peak count filter: 0%; gap filling by compulsion, true. Metabolites were annotated based on the reference standards, including retention time and accurate mass (MS1).

For testing the *Isotope Tracking* module that supports D_2O labeling experiments, MS-DIAL 4.9.221218 (https://zenodo.org/records/12589462 accessed on 29 May 2026) was used with the same settings.

For structure elucidation, MS-FINDER v. 3.73 (https://github.com/systemsomicslab/MsdialWorkbench/releases/tag/MSFINDER-v3.73 accessed on 29 May 2026) [44] was used with the following parameters: mass tolerance (MS1), 0.002 Da; mass tolerance (MS2), 0.002; relative abundance cut-off, 0.1%; LEWIS and SENIOR check, checked; isotopic ratio tolerance, 20%; element ratio check, common range (99.7%); element selection, O, N, P, S; tree depth, 2; local databases, checked.

3. Results and Discussion

3.1. Co-Infusion, Partial, and Full LC-HDX-MS Strategies

Multiple experimental approaches can be used to introduce hydrogen/deuterium exchange during LC-MS analysis, each characterized by distinct advantages and limitations [34]. In post-column co-infusion LC-HDX-MS, D_2O is introduced via a T-union after chromatographic separation, while conventional (unlabeled) mobile phases are used. This approach minimizes shifts in retention time between unlabeled and labeled analyses, simplifying data comparison. However, implementation often requires additional hardware, such as flow splitters, which increases experimental complexity and cost. Exchange efficiency depends strongly on mixing ratios and flow rates [45], and incomplete exchange may occur under high-flow conditions, potentially affecting sensitivity.

Partial LC-HDX-MS is a simpler, more accessible strategy in which only the major mobile-phase solvents are replaced with their deuterated counterparts (e.g., $H_2O \rightarrow D_2O$), whereas the mobile-phase modifiers remain unlabeled. This approach reduces costs and avoids extensive re-optimization of chromatographic methods, but frequently results in incomplete exchange and measurable retention time shifts between unlabeled and labeled runs.

Full LC-HDX-MS involves replacing all mobile-phase components, including both solvents and mobile-phase modifiers, with their deuterated counterparts. Although operationally more demanding and economically more expensive, this strategy typically yields the most complete exchange and facilitates straightforward interpretation. Nonetheless, partially exchanged species often remain detectable at lower abundance and must be considered when interpreting the data.

Figure 1 compares these HDX approaches using a set of 21 compounds containing 2–7 exchangeable hydrogens (Table S1). Post-column addition of D_2O at 100 µL/min to a HILIC effluent flow of 400 µL/min resulted in only limited H/D exchange, with the detection of base peaks for $[M(1D)+D]^+$ ions with one H/D exchange (Figure 1a). Increasing the D_2O post-column flow rate to 400 µL/min improved the extent of exchange and enabled the formation of fully exchanged ions as base peaks for compounds containing 2–3 exchangeable hydrogens. However, compounds with a higher number of exchangeable hydrogens remained incompletely labeled, with $[M(1H,x-1D)+D]^+$ frequently observed as the dominant isotopologue (Figure 1b).

These preliminary experiments were designed to compare the fundamental H/D exchange performance of the three LC-HDX-MS strategies under controlled conditions using representative reference standards with different numbers of exchangeable hydrogen atoms. Because the post-column D_2O co-infusion approach showed limited exchange efficiency even after increasing the D_2O flow rate, the subsequent experimental evaluation focused on partial and full LC-HDX-MS workflows, which provided substantially more complete deuterium incorporation and are more suitable for practical untargeted metabolomics applications.

In contrast, both partial and full HILIC-HDX-ESI(+)-MS configurations achieved near-complete H/D exchange across the evaluated compounds (Figure 1c,d). Nevertheless, the full HILIC-HDX–ESI(+)-MS setup consistently produced a higher abundance of the fully exchanged species, $[M(xD)+D]^+$, accompanied by a lower contribution of the partially exchanged isotopologue $[M(1H,x-1D)+D]^+$. The average absolute intensity difference between these two ions was approximately 20% for the full HILIC-HDX-ESI(+)-MS method, compared with 31% for the partial HILIC-HDX-ESI(+)-MS method. This difference is likely attributable to the presence of non-deuterated mobile-phase additives in the partial HDX configuration, which provides an additional source of exchangeable hydrogen atoms and thereby reduces the formation efficiency of fully deuterated molecular ions.

Similar results were observed for lipidomics, where post-column addition of D_2O to the RPLC effluent resulted in only limited H/D exchange of tested lipids (Table S2) compared with the full RPLC-HDX-ESI(+)-MS workflow (Figure 2).

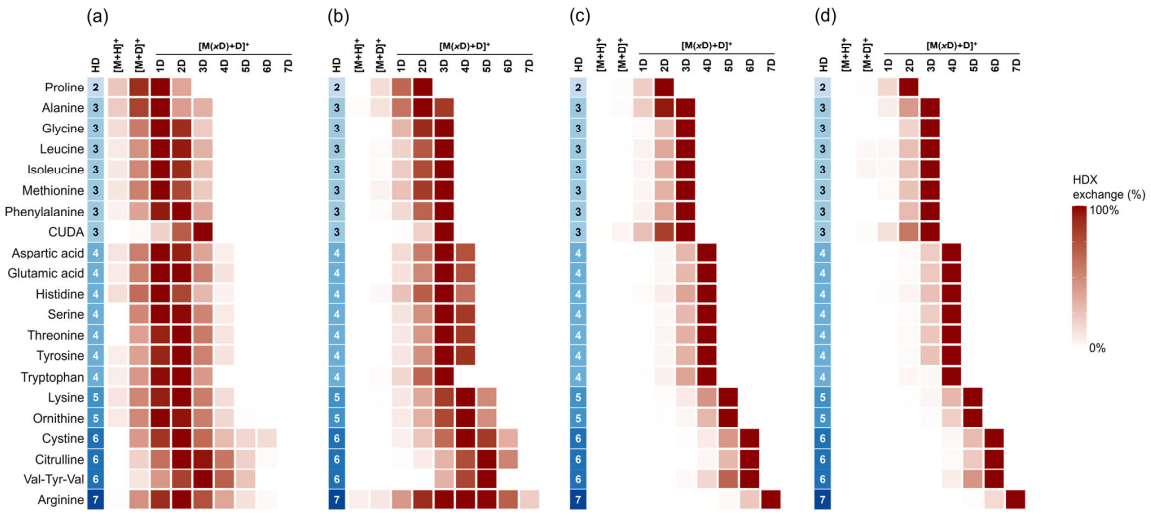

Figure 1. Evaluation of selected target compounds containing 2–7 exchangeable hydrogens using (**a**) conventional HILIC-ESI(+)-MS with post-column addition of D_2O (100 µL/min); (**b**) conventional HILIC-ESI(+)-MS with post-column addition of D_2O (400 µL/min); (**c**) partial HILIC-HDX–ESI(+)-MS with D_2O incorporated into the mobile phases; and (**d**) full HILIC-HDX-ESI(+)-MS with D_2O, ammonium formate-D_5, and formic acid-D_2 incorporated into the mobile phases. The compounds shown were authentic reference standards analyzed as a mixture. In each MS1 spectrum, the most abundant ion (base peak) is shown in dark red, while lower signal intensities are displayed using a proportional color scale. Target compounds are ordered according to the number of exchangeable hydrogens (HD). The chromatographic flow rate was 400 µL/min.

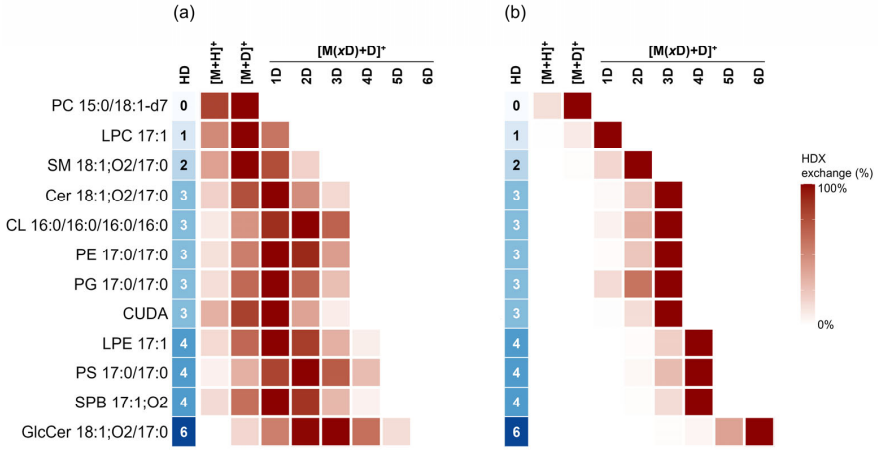

Figure 2. Evaluation of selected target lipids containing 0–6 exchangeable hydrogens using (**a**) conventional lipidomics RPLC-ESI(+)-MS with post-column addition of D_2O (200 µL/min); and (**b**) lipidomics full RPLC-HDX-ESI(+)-MS with D_2O, isopropanol-D_8, ammonium formate-D_5, and formic acid-D_2 incorporated into the mobile phases. The compounds shown were authentic reference standards analyzed as a mixture. In each MS1 spectrum, the most abundant ion (base peak) is shown in dark red, while lower signal intensities are displayed using a proportional color scale. Target compounds are ordered according to the number of exchangeable hydrogens (HD). The chromatographic flow rate was 600 µL/min.

Overall, the evaluated strategies demonstrate that full LC-HDX-MS provides the highest degree of deuterium incorporation, the simplest spectral interpretation, and the greatest confidence in determining the experimentally accessible number of exchangeable hydrogen atoms. Therefore, full LC-HDX-MS is recommended for untargeted small-molecule analysis whenever deuterated mobile phases are available. Nevertheless, practical implementation requires consideration of reagent availability, purity, and cost, which are discussed in the following section.

3.2. Solvent Availability, Purity, and Analytical Consequences

A major practical limitation of LC-HDX-MS is the limited availability of LC-MS-grade deuterated reagents. While unlabeled solvents and additives are widely available at high purity, many deuterated solvents and mobile-phase modifiers are not offered with dedicated LC-MS quality specifications. Therefore, both the chemical purity and isotopic enrichment (atom % D) of deuterated reagents should be considered. In addition, deuterated solvents and additives are available from only a limited number of suppliers (Table S3), and their substantially higher cost may restrict the routine implementation of LC-HDX-MS workflows.

As a consequence, deuterated mobile phases may lead to elevated background signals and retention-time-dependent ion suppression. These effects can substantially influence analytical sensitivity and reproducibility, particularly in untargeted workflows where analytes elute across broad chromatographic windows. Increased background complexity may also compromise data-dependent acquisition (DDA) strategies, necessitating the use of optimized exclusion lists derived from blank injections [46].

Figure 3 illustrates the increase in total ion chromatogram (TIC) intensity observed during LC-HDX-MS experiments. For metabolomics methods (HILIC with D_2O and RPLC with D_2O and methanol-D_4), the TIC increased approximately 2–3-fold relative to the corresponding unlabeled methods. In contrast, lipidomics methods employing isopropanol-D_8 exhibited up to a 10-fold increase in background signal intensity. This observation is consistent with previous reports identifying isopropanol as a particularly challenging solvent for LC-MS-based lipidomic profiling [47]. Even among commercially available LC-MS-grade isopropanol products, substantial differences in background contamination have been observed, with highly abundant mobile-phase impurities, including homologous series of amines, plasticizers, and antioxidant-derived compounds. Such contaminants can generate intense background ions, thereby substantially increasing spectral complexity during analysis [48].

The elevated abundance of background ions can negatively affect mass spectrometric performance. In Orbitrap-based instruments, highly abundant contaminant ions may dominate the ion population accumulated during automatic gain control (AGC). As a result, the AGC target can be reached prematurely, shortening ion injection times and reducing the accumulation of low-abundance analyte ions. This effect can decrease sensitivity and compromise the detection of trace-level metabolites and lipids. Similar concerns apply to time-of-flight (TOF) instruments, where persistent exposure to intense contaminant ions increases the ion flux reaching the microchannel plate detector, potentially accelerating detector aging and reducing long-term instrument performance.

While TIC measurements provide a global assessment of background contamination, they do not directly indicate how analyte signals are affected. Therefore, we next evaluated labeled/unlabeled signal ratios to determine whether the increased background associated with deuterated mobile phases suppresses metabolite and lipid responses. Labeled/unlabeled signal ratios, calculated as the ratio of peak intensities in labeled and unlabeled experiments, revealed signal suppression (ratio < 1) for the majority of compounds (Figure 4). The elevated background signals observed for deuterated mobile phases suggest that increased levels of chemical impurities may contribute to ion suppression by competing with analytes during the ESI process [49]. In addition, deuterated solvents differ from their protonated analogs in several physicochemical properties, including viscosity, surface tension, and hydrogen-bonding behavior, which can influence electrospray droplet formation and desolvation efficiency [50,51]. Consequently, the reduced analyte responses observed under HDX conditions are likely due to both increased background ionization and altered ionization characteristics of the deuterated mobile phases.

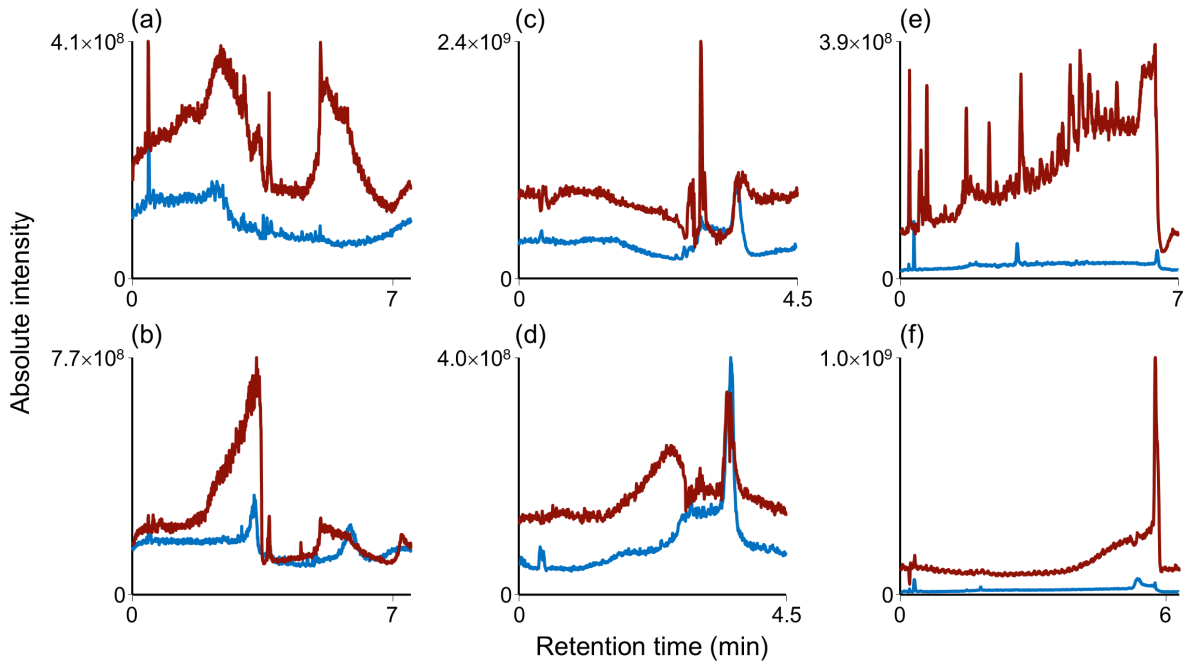

Figure 3. Total ion chromatograms (TICs) of background signals obtained from blank injections using (**a**) metabolomics HILIC-ESI(+)-MS (*m*/*z* 60–900), (**b**) metabolomics HILIC-ESI(–)-MS (*m*/*z* 60–900), (**c**) metabolomics RPLC-ESI(+)-MS (*m*/*z* 60–900), (**d**) metabolomics RPLC-ESI(–)-MS (*m*/*z* 60–900), (**e**) lipidomics RPLC-ESI(+)-MS (*m*/*z* 200–1700), and (**f**) lipidomics RPLC-ESI(–)-MS (*m*/*z* 200–1700). Blue traces correspond to unlabeled mobile phases, whereas red traces correspond to deuterated mobile phases. For each panel, the TIC was normalized to the maximum intensity observed across both conditions.

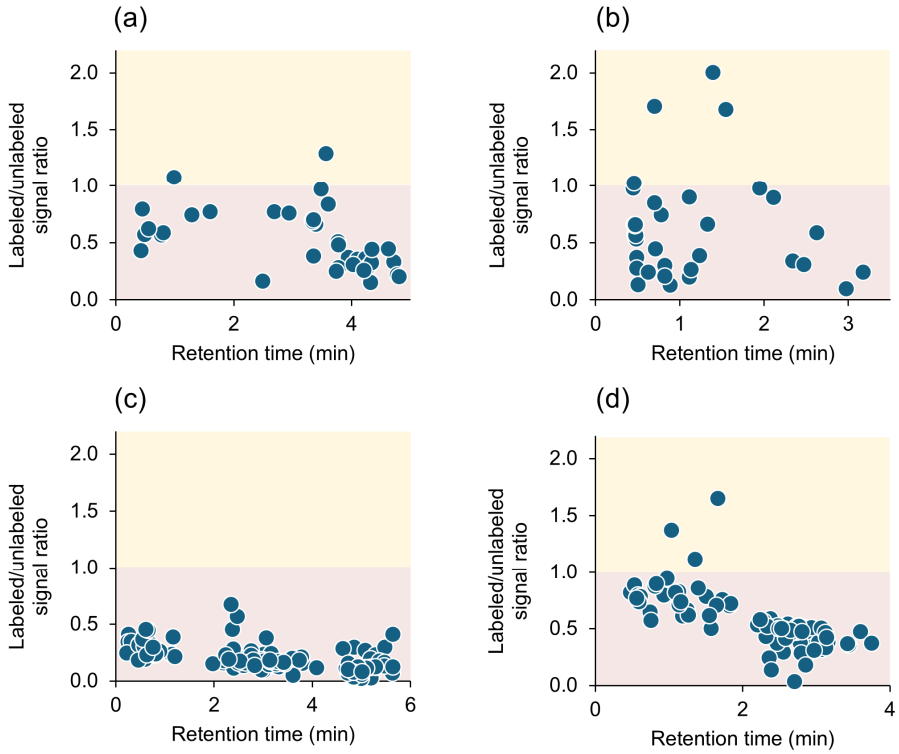

Figure 4. Labeled/unlabeled signal ratios of HDX conditions relative to conventional unlabeled LC-MS conditions for metabolites and exposome compounds detected in NIST SRM 1950 human plasma. Labeled/unlabeled signal ratios were calculated using the peak heights of the fully deuterated molecular ions detected under HDX conditions and the corresponding unlabeled molecular ions detected under conventional LC-MS conditions. Ratios < 1 and >1 correspond to signal suppression

and signal enhancement, respectively. The majority of compounds exhibited ratios below unity, indicating that HDX conditions generally reduced ionization efficiency and/or detection sensitivity. Signal suppression was observed for 89% of compounds detected by (**a**) metabolomics HILIC-ESI(+)-MS, 88% by (**b**) metabolomics RPLC-ESI(−)-MS, 100% by (**c**) lipidomics RPLC-ESI(+)-MS, and 96% by (**d**) lipidomics RPLC-ESI(−)-MS. The number of evaluated compounds was 37, 33, 136, and 119 for panels (**a**–**d**), respectively (Table S4).

From a practical perspective, optimization of both solvent selection and MS acquisition parameters is recommended. Deuterated solvents from different manufacturers should be evaluated, as their impurity profiles may differ substantially. In addition, narrowing the Orbitrap mass acquisition range to the m/z region of interest can reduce premature AGC saturation by background ions, thereby improving ion accumulation for low-abundance analytes and partially mitigating signal suppression.

3.3. Interpretation of HDX Mass Spectra

Interpretation of LC-HDX-MS data requires consideration of exchange efficiency, isotopic distributions, ionization mode, and adduct chemistry [34]. Under optimized LC-HDX-MS conditions, the fully exchanged isotopologue generally dominates the observed isotope distribution. Nevertheless, lower-abundance partially exchanged isotopologues are typically still detected, reflecting incomplete exchange of a small fraction of molecules. Consequently, HDX mass spectra commonly comprise mixtures of fully and partially exchanged species, which should be considered during spectral interpretation and automated feature assignment.

Accurate assignment of HDX-derived features is further complicated by overlap with naturally occurring isotopic peaks, particularly ^{13}C isotopologues. The contribution of these isotopic species depends both on the abundance of partially exchanged ions and on the number of carbon atoms present in the molecule. Although modern high-resolution mass spectrometers readily resolve the mass differences encountered in LC-HDX-MS, correct interpretation still requires consideration of isotopic overlaps and adduct chemistry to avoid misassignment of HDX-derived ions. For example, discrimination between certain HDX-derived ions and overlapping isotopic or adduct-related species separated by approximately 0.003 Da may require resolving powers approaching 100,000 FWHM. In practice, however, partially exchanged isotopologues in full LC-HDX-MS experiments are typically observed at only 10–20% of the intensity of the fully exchanged species [12], limiting the contribution of their ^{13}C isotopologues and minimizing their impact on spectral interpretation.

In addition to the changes observed at the precursor-ion level, LC-HDX-MS may also substantially influence MS/MS fragmentation patterns. During collision-induced dissociation, hydrogen/deuterium redistribution (H/D scrambling) and the elimination of neutral species containing different combinations of hydrogen and deuterium atoms can generate multiple isotopic forms of individual product ions [33,52,53]. Consequently, a single fragment ion observed in the unlabeled experiment may appear as a cluster of fragment ions in the corresponding HDX experiment, differing by approximately one deuterium mass (1.00628 Da). Such fragment-ion clusters should not be confused with naturally occurring ^{13}C isotopic peaks, which are separated by approximately 1.00335 Da. High-resolution mass spectrometry and accurate elemental-composition analysis are therefore essential for the correct interpretation of HDX-derived MS/MS spectra.

The extent of H/D scrambling is compound-dependent and reflects the underlying gas-phase fragmentation mechanism. While some compounds preserve the original deuterium distribution within fragment ions and therefore exhibit only minimal H/D redistribution, others undergo extensive H/D migration during fragmentation, resulting in characteristic fragment-ion clusters. Consequently, HDX-derived MS/MS spectra should not be interpreted simply by shifting fragment masses according to the number of exchanged hydrogen atoms.

Instead, the observed fragmentation patterns should be evaluated in the context of possible H/D redistribution and neutral-loss pathways. Figure 5 illustrates this phenomenon using the amino acid glutamine, where the unlabeled MS/MS spectrum is dominated by individual fragment ions, whereas the corresponding HDX spectrum contains multiple isotopic forms of the same fragments arising from different degrees of deuterium incorporation.

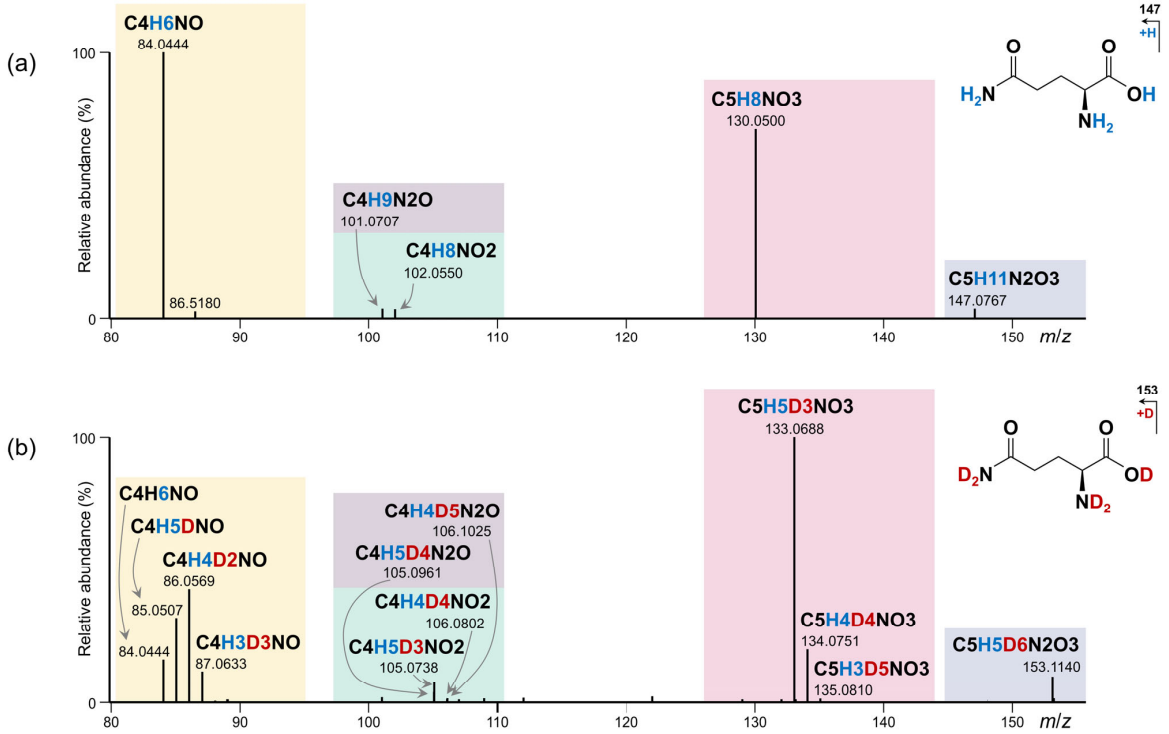

Figure 5. Comparison of MS/MS spectra of the amino acid glutamine acquired using (**a**) conventional HILIC-ESI(+)-MS/MS (precursor ion *m*/*z* 147.0764, $[M(5H)+H]^+$) and (**b**) HILIC-HDX-ESI(+)-MS/MS (precursor ion *m*/*z* 153.1141, $[M(5D)+D]^+$). In the unlabeled experiment, individual fragment ions are observed, whereas the HDX experiment produces characteristic fragment-ion clusters corresponding to different degrees of deuterium incorporation. These clusters arise from H/D redistribution and the elimination of neutral species with different H/D compositions during collision-induced dissociation, illustrating that HDX-derived MS/MS spectra may be substantially more complex than their unlabeled counterparts and therefore require particular attention during spectral interpretation. Assigned elemental compositions are shown with mass accuracies better than 1 mDa. MS/MS spectra were acquired using normalized collision energies of 20%, 30%, and 40%.

Adduct chemistry also influences the interpretation of LC-HDX-MS data [33]. During structural elucidation, correctly assigning the detected ion species is the first step in interpreting LC-MS data. Incorrect ion-species assignment propagates directly into molecular mass determination and subsequent structural annotation, making reliable adduct identification a prerequisite for successful LC-MS-based structure elucidation. Since multiple ion forms are commonly produced during ESI, characteristic mass differences between adducts provide valuable evidence for confirming ion identities. Under HDX conditions, these characteristic mass differences change because exchangeable hydrogen atoms associated with the ion species are replaced by deuterium. Consequently, interpretation of HDX data requires consideration of HDX-specific adduct mass differences rather than those used for conventional LC-MS analysis. Table 1 summarizes the expected mass differences between the most common ion species observed in positive- and negative-ionization modes under both unlabeled and HDX conditions. In negative-ionization mode, loss of a proton from the unlabeled molecular species ($[M(1H)]-H]^-$) and loss of a deuteron from the corresponding fully deuterated molecular species ($[M(1D)]-D]^-$) produce the

same molecular anion. However, because the adduct ions are formed from the fully deuterated molecular species present under HDX conditions, the characteristic mass differences between ion species differ from those observed in conventional LC-MS.

Table 1. Characteristic mass differences between common ion species in conventional LC-MS and LC-HDX-MS experiments.

Ion Mode	Unlabeled LC-MS		HDX-labeled LC-MS	
	Ion Pairs	**Δ*m***	**Ion Pairs**	**Δ*m***
Positive	$+H \leftrightarrow +NH_4$	17.0265	$+D \leftrightarrow +ND_4$	20.0454
	$+H \leftrightarrow +Na$	21.9819	$+D \leftrightarrow +Na$	20.9757
	$+NH_4 \leftrightarrow +Na$	4.9554	$+ND_4 \leftrightarrow +Na$	0.9303
Negative	$-H \leftrightarrow +Cl$	35.9767	$-D \leftrightarrow +Cl$	36.9830
	$-H \leftrightarrow +HCOO$	46.0055	$-D \leftrightarrow +DCOO$	48.0180
	$-H \leftrightarrow +CH_3COO$	60.0211	$-D \leftrightarrow +CD_3COO$	64.0462

Mass differences for HDX-labeled experiments are calculated between ion species derived from the fully deuterated molecular form expected under HDX conditions. They therefore represent characteristic adduct mass differences within the HDX experiment rather than between unlabeled and labeled experiments.

Figure 6 illustrates these effects using cholesteryl ester (CE) 18:2, a lipid that contains no exchangeable hydrogen atoms. Under HDX conditions, conversion of the ammonium adduct from $[M+NH_4]^+$ to $[M+ND_4]^+$ produces a near-isobaric overlap between the ^{13}C isotopologue of $[M+ND_4]^+$ and the $[M+Na]^+$ adduct. Despite this interference, the ions remain baseline resolved at the acquired mass resolution, allowing unambiguous assignment of both species.

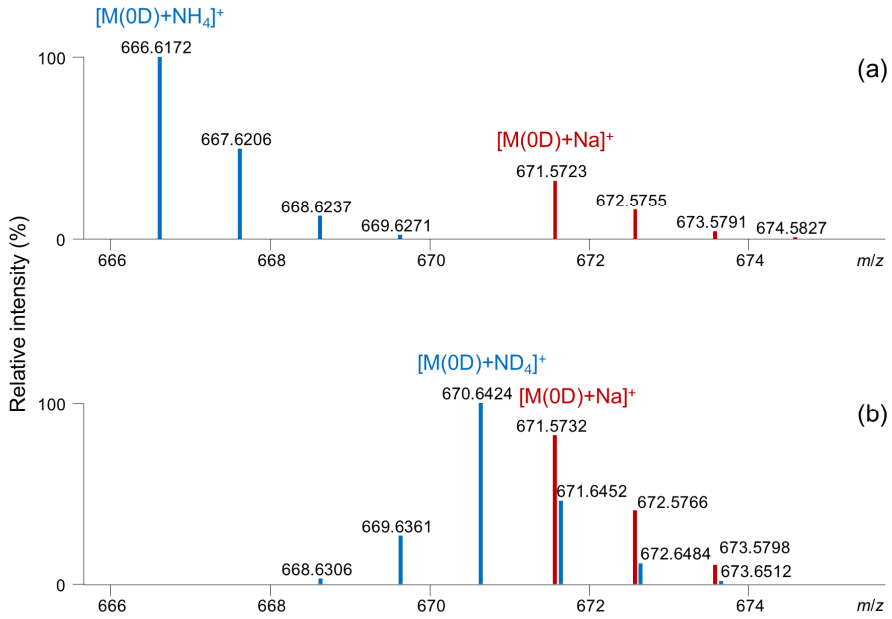

Figure 6. MS1 spectra of cholesteryl ester (CE) 18:2, which contains no exchangeable hydrogen atoms, detected in NIST SRM 1950 during lipidomics RPLC-ESI(+)-MS analysis. In the unlabeled experiment, the ammonium and sodium adducts are well separated. Under HDX conditions, the ammonium adduct $[M+NH_4]^+$ is converted to $[M+ND_4]^+$, resulting in a near-isobaric overlap between the ^{13}C isotopologue of $[M+ND_4]^+$ and the $[M+Na]^+$ adduct. However, at the acquired mass resolution (~22,000 FWHM at m/z 671), the ions remain baseline-resolved, enabling unambiguous differentiation of the two species. (**a**) Unlabeled experiment: $[M+NH_4]^+$ at m/z 666.6172 and $[M+Na]^+$ at m/z 671.5723. (**b**) HDX-labeled experiment: $[M+ND_4]^+$ at m/z 670.6435 and $[M+Na]^+$ at m/z 671.5732. The ^{13}C isotopologue of $[M+ND_4]^+$ is observed at m/z 671.6452.

3.4. Retention-Time Shift Between Unlabeled and Labeled Runs

Partial and full LC-HDX-MS workflows frequently introduce retention-time differences between unlabeled and labeled analyses [33]. These shifts are compound-specific and may vary in both magnitude and direction, reflecting isotope-dependent chromatographic effects. Importantly, partially and fully exchanged isotopologues of the same analyte generally coelute within the labeled run, providing an additional criterion for validating HDX-derived feature assignments.

For metabolites and exposome compounds detected in NIST SRM 1950 human plasma, isotopic substitution had only a modest impact on chromatographic retention, with retention-time differences generally confined to ±0.2 min. Although these shifts were relatively small in absolute terms, they were substantially larger than the normal run-to-run retention-time variability of the corresponding LC-MS methods (typically <0.05 min) and should therefore be considered when matching features between unlabeled and HDX-labeled datasets.

In metabolomics HILIC-ESI(+)-MS, most compounds (89%) exhibited negative retention-time shifts and eluted earlier under HDX conditions (Figure 7a). In contrast, 67% of compounds analyzed by metabolomics RPLC-ESI(−)-MS displayed positive retention-time shifts (Figure 7b). For lipidomics RPLC-ESI(+)-MS and RPLC-ESI(−)-MS analyses (Figure 7c,d), retention-time shifts increased progressively with retention time, reaching approximately +0.2 min for the latest-eluting compounds. Collectively, these results demonstrate that deuterated mobile phases subtly influence chromatographic selectivity and retention behavior, requiring appropriate retention-time tolerances when matching features between unlabeled and HDX-labeled datasets.

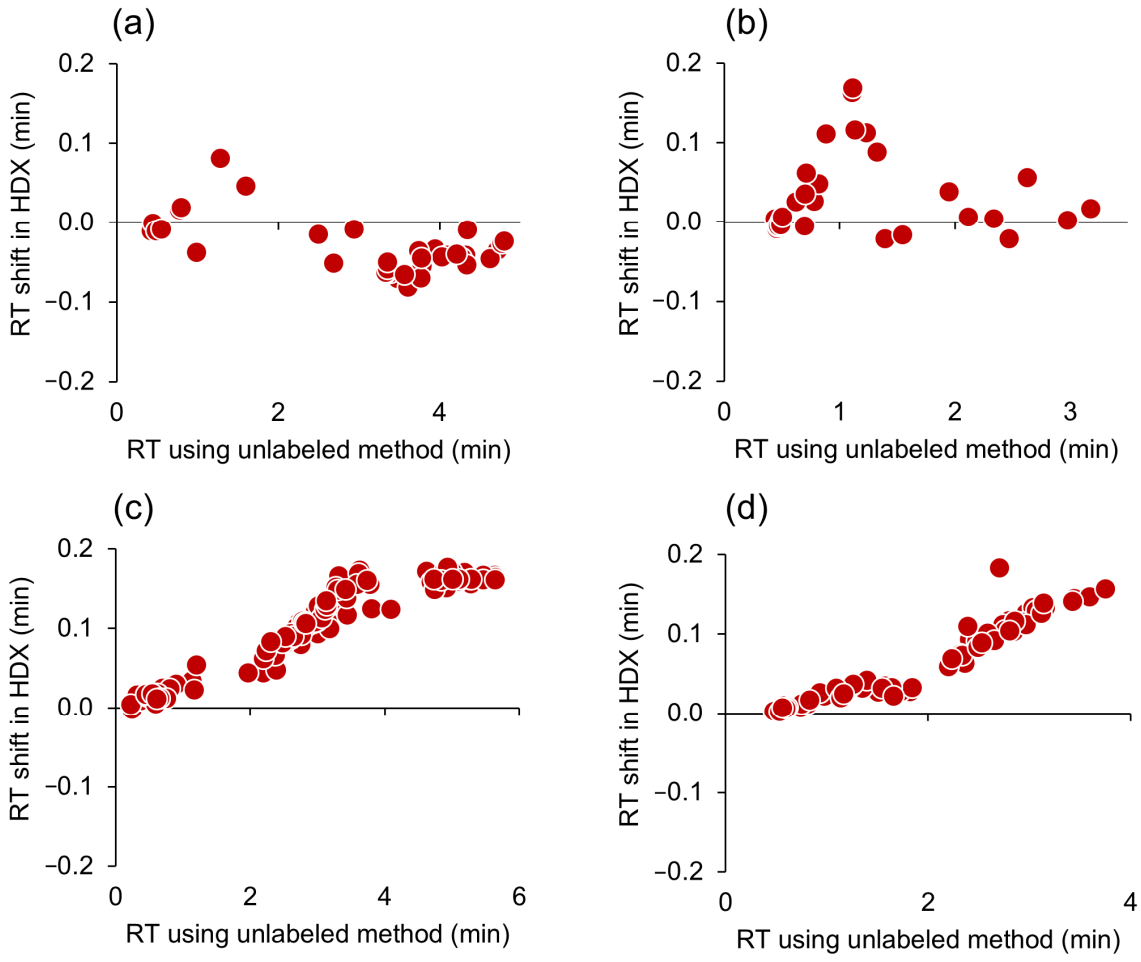

Figure 7. Retention-time shifts between unlabeled and HDX-labeled LC-MS analyses of compounds detected in NIST SRM 1950 human plasma. Each point represents an individual compound and is

plotted according to its RT in the unlabeled analysis and the RT difference between unlabeled and HDX-labeled conditions. Panels show (**a**) metabolomics HILIC-ESI(+)-MS, (**b**) metabolomics RPLC-ESI(−)-MS, (**c**) lipidomics RPLC-ESI(+)-MS, and (**d**) lipidomics RPLC-ESI(−)-MS. Retention-time shifts were generally limited to ±0.2 min, though systematic trends varied across chromatographic modes. The number of evaluated compounds was n = 37, 33, 136, and 119 for panels (**a**–**d**), respectively (Table S4).

3.5. Data Processing and Visualization Workflows

While diverse specialized software exists for protein HDX-MS data analysis [38], equivalent solutions for small-molecule LC-HDX-MS remain largely unavailable. Consequently, metabolomics researchers must often rely on conventional untargeted metabolomics software combined with extensive manual interpretation and custom post-processing workflows.

Conventional metabolomics software platforms, such as MS-DIAL [43] and MZmine [54], provide robust functionality for feature detection, alignment, peak integration, and annotation. However, these platforms were not specifically designed to handle paired unlabeled and HDX-labeled datasets, where multiple isotopologues corresponding to varying numbers of exchanged deuterium atoms must be interpreted together. As a result, visualization and interpretation of HDX experiments frequently require custom workflows and substantial manual validation.

MS-DIAL 5 contains an *Isotope Tracking* module that supports D_2O labeling experiments [43]. However, this functionality is still under active development, and the developers currently recommend using MS-DIAL 4 for isotope-label tracking workflows. In MS-DIAL 4 [55], unlabeled and labeled files can be processed simultaneously, and detected HDX partners are visually linked to their corresponding unlabeled precursors in the *Alignment Spot Viewer* (Figure 8). The software also displays the observed mass shift between the unlabeled and labeled species. Nevertheless, exporting and linking these relationships for downstream interpretation remains largely manual, often requiring additional post-processing scripts or external tools. Furthermore, simultaneous visualization of overlaid extracted ion chromatograms (EICs) for unlabeled and labeled species is not supported.

MZmine can also be adapted for LC-HDX-MS data processing [54]. Following feature detection and alignment, the *Adduct Search* (MZmine 2) module can be used to identify candidate HDX feature pairs by screening for exact mass differences corresponding to one or more deuterium incorporations within a narrow retention-time window. This strategy was previously employed for untargeted screening of HDX-active metabolites, in which detected feature pairs were subsequently manually verified [22]. Although effective for initial discovery, this approach becomes increasingly labor-intensive as datasets grow larger and deuterium incorporation increases. Moreover, increasing isotopic complexity can reduce identification accuracy, necessitating extensive manual review of candidate assignments.

These limitations highlight a broader challenge in translating HDX-derived information into practical structural knowledge: existing software can detect candidate HDX-related features, but provides limited support for integrated interpretation of chromatographic, MS1, and MS/MS evidence. Users frequently need to navigate multiple software environments to validate isotopic relationships, inspect chromatographic co-elution, assess deuterium incorporation patterns, and evaluate fragmentation behavior [22]. The lack of dedicated visualization tools slows data interpretation and increases the risk of overlooking valuable structural information contained within HDX experiments.

To address these challenges, we recently developed ExchangeXplorer [56], an R/Shiny application designed specifically for LC-HDX-MS-guided metabolite characterization. ExchangeXplorer is intended as a complementary post-processing tool that extends conventional LC-MS data analysis with HDX-specific functionality rather than replacing established software for feature detection, alignment, and annotation. The software supports

multiple adduct species, links unlabeled and HDX-derived features based on expected mass differences and retention times, facilitates visualization of isotopic patterns arising from deuterium incorporation, and integrates chromatographic, MS1, and MS/MS evidence within a single interactive environment. Additional information on the software capabilities, documentation, and source code is publicly available [56]. Such dedicated tools are essential for translating HDX-derived information into practical structural insights within untargeted metabolomics workflows.

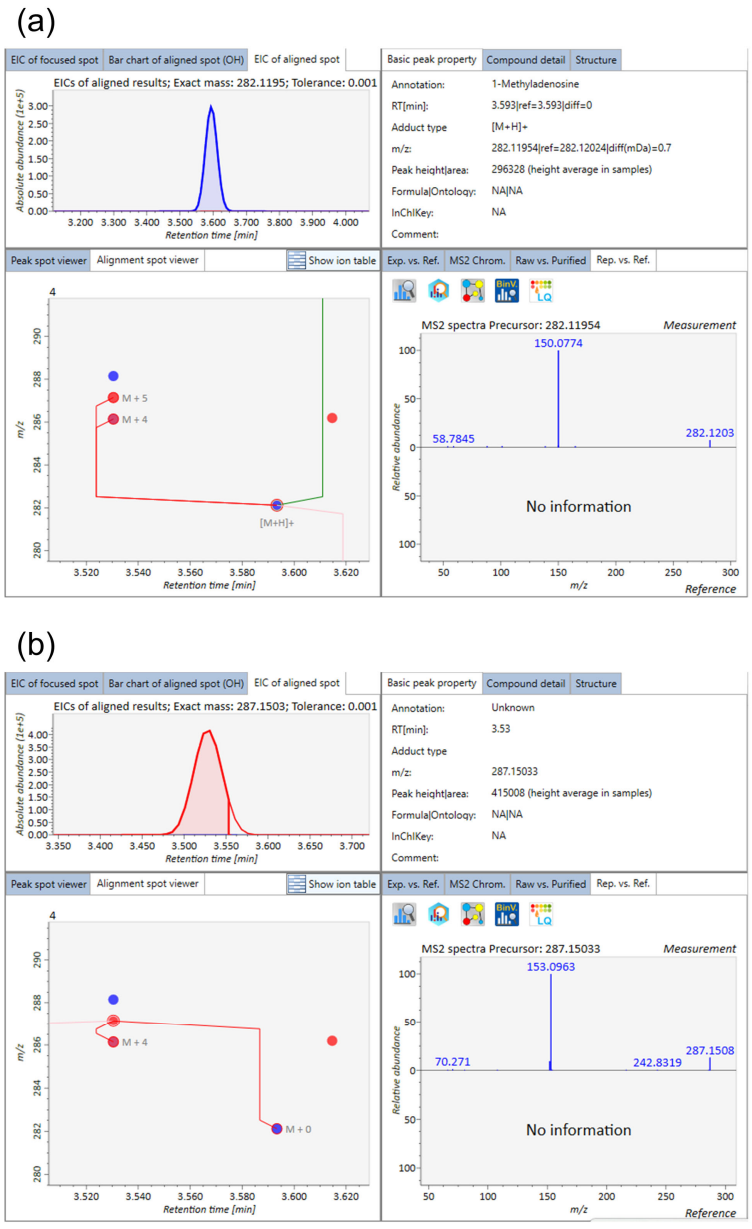

Figure 8. Detection of 1-methyladenosine, containing four exchangeable hydrogen atoms, in human plasma (NIST SRM 1950) and visualization in MS-DIAL 4. 1-Methyladenosine was detected as $[M(4H)+H]^+$ at m/z 282.1197 in the unlabeled experiment (**a**) and as $[M(4D)+D]^+$ at m/z 287.1511 in the HDX-labeled experiment (**b**). In the alignment spot viewer, labeled isotopologues are displayed as M + 4 and M + 5, corresponding to $[M(1H,3D)+D]^+$ at m/z 286.1448 and $[M(4D)+D]^+$ at m/z 287.1511, respectively, relative to the unlabeled species (M + 0). The observed mass shifts reflect the progressive replacement of exchangeable hydrogen atoms by deuterium during HDX labeling.

An example visualization of 1-methyladenosine detected in NIST SRM 1950 human plasma using ExchangeXplorer is shown in Figure 9. The HDX MS/MS Viewer displays

MS1 and MS/MS spectra from both unlabeled and labeled experiments side-by-side, enabling rapid assessment of precursor mass shifts and fragment-ion behavior following deuterium incorporation (Figure 9a). In parallel, the HDX EIC Explorer provides chromatographic validation through overlaid EICs of the unlabeled metabolite and all corresponding HDX partners, facilitating confirmation of co-elution and exchange relationships (Figure 9b). In addition, all results are merged into a single XLSX file that can be directly integrated into downstream annotation workflows. Together, these complementary visualizations enable efficient validation and interpretation of HDX-derived structural information in complex untargeted metabolomics datasets.

Figure 9. Detection of 1-methyladenosine with four exchangeable hydrogens in human plasma (NIST SRM 1950) and visualization in ExchangeXplorer. (**a**) HDX MS/MS Viewer for visualization and comparison of MS1 and MS/MS spectra of unlabeled and HDX-labeled feature pairs. (**b**) HDX EIC

Explorer for extraction and overlay of extracted ion chromatograms (EICs) of an unlabeled feature and all corresponding HDX partners. 1-Methyladenosine was detected as $[M(4H)+H]^+$ at m/z 282.1197 in the unlabeled experiment and as $[M(4D)+D]^+$ at m/z 287.1511 in the labeled experiment. The observed Δm = 5 reflects the total mass shift between unlabeled and labeled ions, including the difference in ion species ($[M+H]^+$ versus $[M+D]^+$). Additional confirmation is provided by the presence of partially unlabeled species ($[M(1H,3D)+D]^+$, m/z 286.1448), which exhibits the same retention time as the fully labeled species ($[M(4D)+D]^+$) but lower signal intensity.

3.6. LC-HDX-MS as an Orthogonal Tool for Structural Elucidation

The principal advantage of LC-HDX-MS lies in its ability to provide orthogonal structural information that complements accurate mass, isotope patterns, retention time, and MS/MS fragmentation. Rather than replacing conventional LC-MS workflows, HDX provides an independent experimental descriptor that increases confidence in structural elucidation and reduces structural ambiguity [57]. By experimentally determining the number of exchangeable hydrogen atoms and refining plausible adduct assignments, LC-HDX-MS can substantially reduce the number of candidate structures generated from accurate mass and fragmentation data alone [33].

To evaluate the theoretical impact of HDX-derived constraints, we used 19 proteinogenic amino acids with 2–7 exchangeable hydrogens as model compounds and assessed the extent to which experimentally determined numbers of exchangeable hydrogens could reduce the pool of candidate structures generated during annotation. Candidate structures were obtained from PubChem (https://pubchem.ncbi.nlm.nih.gov accessed on 26 June 2026) and from MS-FINDER [44]. For PubChem, all structures matching the elemental formula of each amino acid were retrieved, and the number of exchangeable hydrogens was determined from the corresponding molecular structures. For MS-FINDER, candidate structures were generated from LC-MS/MS data using the default internal databases, excluding PubChem Online and MINEs.

For PubChem, an average of 2634 candidate structures per elemental formula was identified, ranging from 158 to 12,231. Incorporation of HDX information eliminated approximately 76% of structures that were inconsistent with the experimentally observed number of exchangeable hydrogens. For MS-FINDER, the number of candidate structures ranged from 2 to 64, and HDX filtering eliminated approximately 60% of candidates.

Although these reductions illustrate the discriminatory power of HDX-derived information, they should not be interpreted as the practical gain achieved in complete annotation workflows. In practice, accurate mass, chromatographic retention, MS/MS fragmentation, isotope patterns, adduct assignment, and biological context already eliminate many implausible candidates before HDX information is considered. Rather, HDX provides an additional orthogonal experimental constraint by experimentally determining the number of exchangeable hydrogen atoms, thereby further increasing confidence in the remaining structural assignments and reducing the likelihood of false-positive annotations. This complementary value is particularly relevant for compounds that remain ambiguous after conventional LC-MS analysis, where HDX-derived information can provide an additional level of experimental evidence during structural annotation [58].

The utility of LC-HDX-MS has been demonstrated in our recent biological applications, including studies of dietary and microbiome interventions in mice [12], circadian metabolomics across multiple rat tissues [40], and clinical metabolomics investigations aimed at discovering biomarkers of metformin adherence [41] and characterizing metabolites in human lung cancer [59].

In these studies, HDX-derived information was interpreted alongside accurate mass, retention time, adduct assignment, and MS/MS fragmentation to increase confidence in structural annotation. For example, during the annotation of N^1-acetylspermidine,

the experimentally observed number of exchangeable hydrogen atoms eliminated 78% of false-positive candidate structures generated from accurate mass alone, providing an additional level of confidence in the final structural assignment [12]. Similar benefits were observed during the characterization of N-lactoyl-amino acids, where HDX-derived information served as an additional orthogonal experimental constraint for evaluating candidate structures [41]. Collectively, these studies demonstrate that LC-HDX-MS is not intended to replace conventional annotation workflows. Rather, it provides complementary experimental evidence that is particularly valuable for compounds remaining ambiguously annotated after conventional LC-MS analysis, where accurate mass, retention time, adduct assignment, isotope patterns, and MS/MS fragmentation alone are insufficient for confident structural assignment.

4. Conclusions

LC-HDX-MS provides an orthogonal source of experimental structural information that complements conventional LC-MS and improves confidence in small-molecule structural elucidation. Our experimental evaluation demonstrates that full HDX workflows generally achieve the most complete deuterium incorporation and facilitate simpler data interpretation, whereas deuterated mobile phases can increase background signals and reduce analyte responses. Although retention-time shifts between unlabeled and HDX-labeled analyses are typically modest, they should be considered during feature matching and data processing.

By experimentally determining the number of exchangeable hydrogen atoms and refining adduct assignments, LC-HDX-MS provides additional structural descriptors that substantially reduce ambiguity during structural elucidation. LC-HDX-MS should therefore not be viewed as a replacement for accurate-mass and MS/MS-based workflows, but rather as an orthogonal analytical approach that complements conventional LC-MS by providing independent experimental evidence for structural assignment. Its greatest value is expected for compounds that remain ambiguously annotated after conventional LC-MS analysis, where HDX-derived information can serve as an additional experimental constraint alongside accurate mass, retention time, isotope patterns, adduct assignment, and MS/MS fragmentation. Accordingly, LC-HDX-MS is best viewed as a targeted follow-up strategy for selected metabolites that remain ambiguously annotated after conventional untargeted LC-MS analysis, rather than as a routine workflow for every untargeted metabolomics experiment. Consequently, LC-HDX-MS is particularly well suited for targeted structural investigations, characterization of unknown metabolites, and applications requiring the highest possible confidence in small-molecule identification.

Supplementary Materials: The following supporting information can be downloaded at https://www.mdpi.com/article/10.3390/analytica7030057/s1, Table S1: Target compounds evaluated using metabolomics HILIC-ESI(+)-MS; Table S2: Target compounds evaluated using lipidomics RPLC-ESI(+)-MS; Table S3: Examples of solvents and modifiers for LC-HDX-MS; Table S4: Metabolites and exposome compounds detected in NIST SRM 1950 human plasma for HDX evaluation.

Author Contributions: Conceptualization, T.C. and O.F.; methodology, T.C. and O.F.; software, T.C. and M.N.; validation, T.C.; formal analysis, T.C.; investigation, T.C., J.H., L.R.K., V.H., M.P., M.N. and O.F.; resources, T.C.; data curation, T.C.; writing—original draft preparation, T.C.; writing—review and editing, T.C. and O.F.; visualization, T.C.; supervision, T.C.; project administration, T.C.; funding acquisition, T.C. All authors have read and agreed to the published version of the manuscript.

Funding: This research was funded by the Czech Science Foundation (21-00477S).

Data Availability Statement: The data are contained within this article and in the Supplementary Materials.

Acknowledgments: The data were acquired at the Metabolomics Core Facility (https://metabolomics.fgu.cas.cz/ accessed on 26 June 2026) at the Institute of Physiology of the Czech Academy of Sciences.

Conflicts of Interest: The authors declare no conflicts of interest.

References

1. Dettmer, K.; Aronov, P.A.; Hammock, B.D. Mass spectrometry-based metabolomics. *Mass Spectrom. Rev.* **2007**, *26*, 51–78. [CrossRef] [PubMed]
2. Castro-Alves, V.; Nguyen, A.H.; Barbosa, J.M.G.; Oresic, M.; Hyotylainen, T. Liquid and gas-chromatography-mass spectrometry methods for exposome analysis. *J. Chromatogr. A* **2025**, *1744*, 465728. [CrossRef] [PubMed]
3. Zullig, T.; Trotzmuller, M.; Kofeler, H.C. Lipidomics from sample preparation to data analysis: A primer. *Anal. Bioanal. Chem.* **2020**, *412*, 2191–2209. [CrossRef] [PubMed]
4. O'Shea, K.; Misra, B.B. Software tools, databases and resources in metabolomics: Updates from 2018 to 2019. *Metabolomics* **2020**, *16*, 36. [CrossRef] [PubMed]
5. Nafie, M.S.; Abu-Elsaoud, A.M.; Diab, M.K. A comprehensive review on computational metabolomics: Advancing multiscale analysis through in-silico approaches. *Comput. Struct. Biotechnol. J.* **2025**, *27*, 3191–3215. [CrossRef] [PubMed]
6. Beniddir, M.A.; Kang, K.B.; Genta-Jouve, G.; Huber, F.; Rogers, S.; van der Hooft, J.J.J. Advances in decomposing complex metabolite mixtures using substructure- and network-based computational metabolomics approaches. *Nat. Prod. Rep.* **2021**, *38*, 1967–1993. [CrossRef] [PubMed]
7. Domingo-Fernandez, D.; Healey, D.; Kind, T.; Allen, A.; Colluru, V.; Misra, B.B. Trends in Computational Metabolomics: A Perspective on Five Years of Software Development, Challenges, and Opportunities (2021–2025). *Anal. Chem.* **2026**, *98*, 19962–19974. [CrossRef] [PubMed]
8. Kapse, B.P.; Soni, R.P. Evolving LC-MS hyphenations: Strengths, limitations, and emerging trends in bioanalytical applications. *Talanta* **2026**, *308*, 129759. [CrossRef] [PubMed]
9. de Jonge, N.F.; Mildau, K.; Meijer, D.; Louwen, J.J.R.; Bueschl, C.; Huber, F.; van der Hooft, J.J.J. Good practices and recommendations for using and benchmarking computational metabolomics metabolite annotation tools. *Metabolomics* **2022**, *18*, 103. [CrossRef] [PubMed]
10. James, E.I.; Murphree, T.A.; Vorauer, C.; Engen, J.R.; Guttman, M. Advances in Hydrogen/Deuterium Exchange Mass Spectrometry and the Pursuit of Challenging Biological Systems. *Chem. Rev.* **2022**, *122*, 7562–7623. [CrossRef] [PubMed]
11. Hamuro, Y. Tutorial: Chemistry of Hydrogen/Deuterium Exchange Mass Spectrometry. *J. Am. Soc. Mass Spectrom.* **2021**, *32*, 133–151. [CrossRef] [PubMed]
12. Cajka, T.; Hricko, J.; Rakusanova, S.; Brejchova, K.; Novakova, M.; Rudl Kulhava, L.; Hola, V.; Paucova, M.; Fiehn, O.; Kuda, O. Hydrophilic Interaction Liquid Chromatography-Hydrogen/Deuterium Exchange-Mass Spectrometry (HILIC-HDX-MS) for Untargeted Metabolomics. *Int. J. Mol. Sci.* **2024**, *25*, 2899. [CrossRef] [PubMed]
13. Fischer, C.R.; Wilmes, P.; Bowen, B.P.; Northen, T.R.; Banfield, J.F. Deuterium-exchange metabolomics identifies N-methyl lyso phosphatidylethanolamines as abundant lipids in acidophilic mixed microbial communities. *Metabolomics* **2012**, *8*, 566–578. [CrossRef]
14. Lam, W.; Ramanathan, R. In electrospray ionization source hydrogen/deuterium exchange LC-MS and LC-MS/MS for characterization of metabolites. *J. Am. Soc. Mass Spectrom.* **2002**, *13*, 345–353. [CrossRef] [PubMed]
15. Liu, D.Q.; Wu, L.; Sun, M.; MacGregor, P.A. On-line H/D exchange LC-MS strategy for structural elucidation of pharmaceutical impurities. *J. Pharm. Biomed. Anal.* **2007**, *44*, 320–329. [CrossRef] [PubMed]
16. Liu, D.Q.; Hop, C.E. Strategies for characterization of drug metabolites using liquid chromatography-tandem mass spectrometry in conjunction with chemical derivatization and on-line H/D exchange approaches. *J. Pharm. Biomed. Anal.* **2005**, *37*, 1–18. [CrossRef] [PubMed]
17. Pfeifer, T.; Tuerk, J.; Fuchs, R. Structural characterization of sulfadiazine metabolites using H/D exchange combined with various MS/MS experiments. *J. Am. Soc. Mass Spectrom.* **2005**, *16*, 1687–1694. [CrossRef] [PubMed]
18. Williamson, D.L.; Trimble, T.K.; Nagy, G. Hydrogen-Deuterium-Exchange-Based Mass Distribution Shifts in High-Resolution Cyclic Ion Mobility Separations. *J. Am. Soc. Mass Spectrom.* **2023**, *34*, 1024–1034. [CrossRef] [PubMed]
19. Shi, C.; Jia, H.; Chen, S.; Huang, J.; Peng, Y.; Guo, W. Hydrogen/Deuterium Exchange Aiding Metabolite Identification in Single-Cell Nanospray High-Resolution Mass Spectrometry Analysis. *Anal. Chem.* **2022**, *94*, 650–657. [CrossRef] [PubMed]
20. Bloszies, C.S. Expanding Coverage of the Chemical Exposome Using Novel Data Acquisition and Computational Tools. Ph.D. Thesis, University of California, Davis, CA, USA, 2020.
21. Christopher, M.W.; Prentice, B.M.; Garrett, T.J. Distinguishing 4- vs 5-Hydroxy-N,N-Dimethyltryptamine (Psilocin vs Bufotenine) Using Hydrogen-Deuterium Back-Exchange. *J. Am. Soc. Mass Spectrom.* **2026**, *37*, 570–573. [CrossRef] [PubMed]

22. Christopher, M.W.; Ericson, A.C.; Guo, Y.; Beauchamp, G.C.; Prentice, B.M.; Garrett, T.J. Hydrogen-Deuterium Back-Exchange for High-Resolution Mass-Spectrometry-Based Metabolite Characterization. *Anal. Chem.* **2026**, *98*, 18432–18442. [CrossRef] [PubMed]
23. Song, X.; Li, J.; Mofidfar, M.; Zare, R.N. Distinguishing between Isobaric Ions Using Microdroplet Hydrogen-Deuterium Exchange Mass Spectrometry. *Metabolites* **2021**, *11*, 728. [CrossRef] [PubMed]
24. Christopher, M.W.; Ericson, A.C.; Klug, A.C.; Dinglasan, R.R.; Prentice, B.M.; Garrett, T.J. Divergent Metabolic Fates of Aromatic Amino Acid-Derived Isomers: Insights from Ex Vivo Metabolomics and HDX-HRMS/MS-Based Resolution of Tautomers. *Anal. Chem.* **2024**, *96*, 16917–16925. [CrossRef] [PubMed]
25. Majuta, S.N.; Li, C.; Jayasundara, K.; Kiani Karanji, A.; Attanayake, K.; Ranganathan, N.; Li, P.; Valentine, S.J. Rapid Solution-Phase Hydrogen/Deuterium Exchange for Metabolite Compound Identification. *J. Am. Soc. Mass Spectrom.* **2019**, *30*, 1102–1114. [CrossRef] [PubMed]
26. Freitas, M.A.; Shi, S.D.H.; Hendrickson, C.L.; Marshall, A.G. Gas-Phase RNA and DNA Ions. 1. H/D Exchange of the $[M - H]^-$ Anions of Nucleoside 5'-Monophosphates (GMP, dGMP, AMP, dAMP, CMP, dCMP, UMP, dTMP), Ribose 5-Monophosphate, and 2-Deoxyribose 5-Monophosphate with D2O and D2S. *J. Am. Chem. Soc.* **1998**, *120*, 10187–10193. [CrossRef]
27. Eysseric, E.; Bellerose, X.; Lavoie, J.M.; Segura, P.A. Post-column hydrogen-deuterium exchange technique to assist in the identification of small organic molecules by mass spectrometry. *Can. J. Chem.* **2016**, *94*, 781–787. [CrossRef]
28. Jansson, E.T.; Lai, Y.H.; Santiago, J.G.; Zare, R.N. Rapid Hydrogen-Deuterium Exchange in Liquid Droplets. *J. Am. Chem. Soc.* **2017**, *139*, 6851–6854. [CrossRef] [PubMed]
29. Uppal, S.S.; Mookherjee, A.; Harkewicz, R.; Beasley, S.E.; Bush, M.F.; Guttman, M. High-Precision, Gas-Phase Hydrogen/Deuterium-Exchange Kinetics by Mass Spectrometry Enabled by Exchange Standards. *Anal. Chem.* **2020**, *92*, 7725–7732. [CrossRef] [PubMed]
30. Robinson, J.M.; Greig, M.J.; Griffey, R.H.; Mohan, V.; Laude, D.A. Hydrogen/deuterium exchange of nucleotides in the gas phase. *Anal. Chem.* **1998**, *70*, 3566–3571. [CrossRef] [PubMed]
31. Rensner, J.J.; Lee, Y.J. Efficient Hydrogen-Deuterium Exchange in Matrix-Assisted Laser Desorption/Ionization Mass Spectrometry Imaging for Confident Metabolite Identification. *Anal. Chem.* **2022**, *94*, 11129–11133. [CrossRef] [PubMed]
32. Song, X.; Zang, Q.; Zare, R.N. Hydrogen-Deuterium Exchange Desorption Electrospray Ionization Mass Spectrometry Visualizes an Acidic Tumor Microenvironment. *Anal. Chem.* **2021**, *93*, 10411–10417. [CrossRef] [PubMed]
33. Ruttkies, C.; Schymanski, E.L.; Strehmel, N.; Hollender, J.; Neumann, S.; Williams, A.J.; Krauss, M. Supporting non-target identification by adding hydrogen deuterium exchange MS/MS capabilities to MetFrag. *Anal. Bioanal. Chem.* **2019**, *411*, 4683–4700. [CrossRef] [PubMed]
34. Damont, A.; Legrand, A.; Cao, C.; Fenaille, F.; Tabet, J.C. Hydrogen/deuterium exchange mass spectrometry in the world of small molecules. *Mass Spectrom. Rev.* **2023**, *42*, 1300–1331. [CrossRef] [PubMed]
35. Kim, P.; Continetti, R.E. Accelerated Keto-Enol Tautomerization Kinetics of Malonic Acid in Aqueous Droplets. *ACS Earth Space Chem.* **2021**, *5*, 2212–2222. [CrossRef]
36. Hatvany, J.B.; Liyanage, O.T.; Gallagher, E.S. Effect of pH on In-Electrospray Hydrogen/Deuterium Exchange of Carbohydrates and Peptides. *J. Am. Soc. Mass Spectrom.* **2024**, *35*, 441–448. [CrossRef] [PubMed]
37. Kostyukevich, Y.; Vladimirov, G.; Stekolschikova, E.; Ivanov, D.; Yablokov, A.; Zherebker, A.; Sosnin, S.; Orlov, A.; Fedorov, M.; Khaitovich, P.; et al. Hydrogen/Deuterium Exchange Aiding Compound Identification for LC-MS and MALDI Imaging Lipidomics. *Anal. Chem.* **2019**, *91*, 13465–13474. [CrossRef] [PubMed]
38. Stofella, M.; Grimaldi, A.; Smit, J.H.; Claesen, J.; Paci, E.; Sobott, F. Computational Tools for Hydrogen-Deuterium Exchange Mass Spectrometry Data Analysis. *Chem. Rev.* **2024**, *124*, 12242–12263. [CrossRef] [PubMed]
39. Cajka, T.; Hricko, J.; Rudl Kulhava, L.; Paucova, M.; Novakova, M.; Kuda, O. Optimization of Mobile Phase Modifiers for Fast LC-MS-Based Untargeted Metabolomics and Lipidomics. *Int. J. Mol. Sci.* **2023**, *24*, 1987. [CrossRef] [PubMed]
40. Rudl Kulhava, L.; Houdek, P.; Novakova, M.; Hricko, J.; Paucova, M.; Kuda, O.; Sladek, M.; Fiehn, O.; Sumova, A.; Cajka, T. Circadian ontogenetic metabolomics atlas: An interactive resource with insights from rat plasma, tissues, and feces. *Cell. Mol. Life Sci.* **2025**, *82*, 264. [CrossRef] [PubMed]
41. Cajka, T.; Hricko, J.; Rudl Kulhava, L.; Paucova, M.; Novakova, M.; Hola, V.; Rakusanova, S.; Fiehn, O.; Skop, V.; Lankova, I.; et al. Untargeted Metabolomics Identifies N-Lactoyl-Amino Acids as Dose-Responsive Plasma Biomarkers of Metformin Adherence in Type 2 Diabetes. *Clin. Pharmacol. Ther.* **2026**, *119*, 1057–1069. [CrossRef] [PubMed]
42. Chambers, M.C.; Maclean, B.; Burke, R.; Amodei, D.; Ruderman, D.L.; Neumann, S.; Gatto, L.; Fischer, B.; Pratt, B.; Egertson, J.; et al. A cross-platform toolkit for mass spectrometry and proteomics. *Nat. Biotechnol.* **2012**, *30*, 918–920. [CrossRef] [PubMed]
43. Takeda, H.; Matsuzawa, Y.; Takeuchi, M.; Takahashi, M.; Nishida, K.; Harayama, T.; Todoroki, Y.; Shimizu, K.; Sakamoto, N.; Oka, T.; et al. MS-DIAL 5 multimodal mass spectrometry data mining unveils lipidome complexities. *Nat. Commun.* **2024**, *15*, 9903. [CrossRef] [PubMed]

44. Tsugawa, H.; Kind, T.; Nakabayashi, R.; Yukihira, D.; Tanaka, W.; Cajka, T.; Saito, K.; Fiehn, O.; Arita, M. Hydrogen Rearrangement Rules: Computational MS/MS Fragmentation and Structure Elucidation Using MS-FINDER Software. *Anal. Chem.* **2016**, *88*, 7946–7958. [CrossRef] [PubMed]
45. Shah, R.P.; Garg, A.; Putlur, S.P.; Wagh, S.; Kumar, V.; Rao, V.; Singh, S.; Mandlekar, S.; Desikan, S. Practical and economical implementation of online H/D exchange in LC-MS. *Anal. Chem.* **2013**, *85*, 10904–10912. [CrossRef] [PubMed]
46. Defossez, E.; Bourquin, J.; von Reuss, S.; Rasmann, S.; Glauser, G. Eight key rules for successful data-dependent acquisition in mass spectrometry-based metabolomics. *Mass Spectrom. Rev.* **2023**, *42*, 131–143. [CrossRef] [PubMed]
47. Cajka, T.; Hricko, J.; Rudl Kulhava, L.; Paucova, M.; Novakova, M.; Fiehn, O.; Kuda, O. Exploring the Impact of Organic Solvent Quality and Unusual Adduct Formation during LC-MS-Based Lipidomic Profiling. *Metabolites* **2023**, *13*, 966. [CrossRef] [PubMed]
48. Roberts, J.A.; Radnoff, A.S.; Bushueva, A.; Menard, J.A.; Wasslen, K.V.; Harley, M.; Manthorpe, J.M.; Smith, J.C. Mobile Phase Contaminants Affect Neutral Lipid Analysis in LC-MS-Based Lipidomics Studies. *J. Am. Soc. Mass Spectrom.* **2024**, *35*, 3095–3106. [CrossRef] [PubMed]
49. Herath, H.M.; Shaw, P.N.; Cabot, P.; Hewavitharana, A.K. Effect of ionization suppression by trace impurities in mobile phase water on the accuracy of quantification by high-performance liquid chromatography/mass spectrometry. *Rapid Commun. Mass Spectrom.* **2010**, *24*, 1502–1506. [CrossRef] [PubMed]
50. Kebarle, P.; Verkerk, U.H. Electrospray: From ions in solution to ions in the gas phase, what we know now. *Mass Spectrom. Rev.* **2009**, *28*, 898–917. [CrossRef] [PubMed]
51. Cech, N.B.; Enke, C.G. Practical implications of some recent studies in electrospray ionization fundamentals. *Mass Spectrom. Rev.* **2001**, *20*, 362–387. [CrossRef] [PubMed]
52. Kuck, D. Scrambling versus specific processes in gaseous organic ions during mass spectrometric fragmentation: Elucidation of mechanistic origins by isotope labelling—An overview. *J. Label. Compd. Rad.* **2007**, *50*, 360–365. [CrossRef]
53. Zheng, S.J.; Zheng, J.; Xiong, C.F.; Xiao, H.M.; Liu, S.J.; Feng, Y.Q. Hydrogen-Deuterium Scrambling Based on Chemical Isotope Labeling Coupled with LC-MS: Application to Amine Metabolite Identification in Untargeted Metabolomics. *Anal. Chem.* **2020**, *92*, 2043–2051. [CrossRef] [PubMed]
54. Heuckeroth, S.; Damiani, T.; Smirnov, A.; Mokshyna, O.; Brungs, C.; Korf, A.; Smith, J.D.; Stincone, P.; Dreolin, N.; Nothias, L.F.; et al. Reproducible mass spectrometry data processing and compound annotation in MZmine 3. *Nat. Protoc.* **2024**, *19*, 2597–2641. [CrossRef] [PubMed]
55. Tsugawa, H.; Ikeda, K.; Takahashi, M.; Satoh, A.; Mori, Y.; Uchino, H.; Okahashi, N.; Yamada, Y.; Tada, I.; Bonini, P.; et al. A lipidome atlas in MS-DIAL 4. *Nat. Biotechnol.* **2020**, *38*, 1159–1163. [CrossRef] [PubMed]
56. Cajka, T. ExchangeXplorer, v. 1.0.0. Available online: https://github.com/tomascajka/ExchangeXplorer (accessed on 26 June 2026).
57. Zhang, Q.; Ford, L.A.; Evans, A.M.; Toal, D.R. Structure elucidation of metabolite x17299 by interpretation of mass spectrometric data. *Metabolomics* **2017**, *13*, 92. [CrossRef] [PubMed]
58. Kind, T.; Tsugawa, H.; Cajka, T.; Ma, Y.; Lai, Z.; Mehta, S.S.; Wohlgemuth, G.; Barupal, D.K.; Showalter, M.R.; Arita, M.; et al. Identification of small molecules using accurate mass MS/MS search. *Mass Spectrom. Rev.* **2018**, *37*, 513–532. [CrossRef] [PubMed]
59. Tietzova, I.; Hricko, J.; Rancourt, R.C.; Schneider, M.A.; Allgauer, M.; Cajka, T. A metabolomics and lipidomics atlas of pulmonary large cell neuroendocrine carcinoma. *Biomed. Pharmacother.* **2026**, *198*, 119327. [CrossRef] [PubMed]